miR-144 delivered by nasopharyngeal carcinoma-derived EVs stimulates angiogenesis through the FBXW7/HIF-1α/VEGF-A axis

Xiaoyan Tian,[1] Yuehui Liu,[1] Zhi Wang,[1] and Shuhong Wu[1]

[1]Department of Otorhinolaryngology Head and Neck Surgery, The Second Affiliated Hospital of Nanchang University, Nanchang 330006, Jiangxi Province, P.R. China

The current study aimed to explore the role of tumor-derived extracellular vesicles (EVs) in angiogenesis during nasopharyngeal carcinoma (NPC). NPC biopsy specimens were initially collected. Human umbilical vein endothelial cells (HUVECs) were co-cultured with EVs isolated from NPC cells, after which their migration, invasion, as well as vessel-like tube formation were evaluated by Transwell chamber systems and Matrigel-based angiogenesis assays. The pro-angiogenic activities of EVs as well as the candidate microRNA (miRNA or miR) were examined using an *in vivo* Matrigel angiogenesis model. The results indicated that the levels of miR-144 in the NPC tissues were upregulated when compared to the nasopharyngeal normal tissues in addition to the identification of a positive correlation with the expression of CD31. Moreover, our data indicated that miR-144 was highly enriched in EVs from NPC cells and then ultimately enhanced the migration and invasion of HUVECs and vessel-like tubes *in vitro* and *in vivo*. Notably, miR-144 was identified as a mediator in NPC-EV-induced regulatory effects through the inhibition of the target gene FBXW7 and promotion of the transcriptional factor HIF-1α-dependent vascular endothelial growth factor (VEGF-A). Taken together, the key findings of the current study highlighted the role of miR-144 as an extracellular pro-angiogenic mediator in NPC tumorigenesis.

INTRODUCTION

Nasopharyngeal carcinoma (NPC), an epithelial malignancy, is prevalent in southeast Asia, is particularly common in Southern China, and is often accompanied by cervical node metastasis.[1] In 2018, newly diagnosed NPC cases accounted for approximately 0.7% of all cancers, as well as 0.8% of cancer deaths on a global scale.[2] Despite significant advances in relation to prevention of NPC local spread through the use of various approaches, including intensity-modulated radiotherapy and optimization of chemotherapy strategies, the management of NPC metastasis remains largely unsatisfactory.[3] Pathological angiogenesis is a fundamental factor for tumor progression and metastasis. Tumor cells release substantial pro-angiogenic factors, which leads to the formation of abnormal disorganized vascular networks in addition to immature and permeable blood vessels, resulting in impaired tumor perfusion.[4] Limited tumor perfusion and the subsequent hypoxic microenvironment can facilitate the survival of more invasive and aggressive tumor cells, while simultaneously inhibiting the tumor-killing action of the immune cells.[5] Recently, the potential role of angiogenesis as a therapeutic target for NPC has been emphasized due to the evidence that irradiation with the coordinated anti-angiogenesis could enhance the antitumor effect on NPC.[6,7] Tumor angiogenesis serves as the hallmark of tumors in an advanced form, which is also observed in NPC.[8] Thus, further studies with a particular emphasis on the angiogenic mechanisms associated with NPC and its molecular drivers are required in order to develop novel therapeutics for NPC.

Extracellular vesicles (EVs) are a class of membrane-enclosed and nano-sized cellular vesicles that are secreted from various cell types, including normal and pathological cells.[9] EVs have been well documented to be significant mediators of cell-cell communication by transferring proteins, lipids, and nucleic acids (mRNA, non-coding RNAs, and DNA).[10] Tumor-derived EVs mediate intercellular communication between tumor cells and stromal cells, creating a tumor microenvironment and a pre-metastatic niche.[11,12] Accumulating evidence continues to suggest that EVs stimulate angiogenesis by means of facilitating tumor-to-endothelial-cell communication in solid tumors, including head and neck squamous cell carcinoma.[13] Existing cancer literature has provided evidence further attesting to the idea that microRNA (miRNA or miR)-enclosed EVs derived from tumor cells could be transferred into endothelial cells and could facilitate their migration and tube formation, ultimately triggering angiogenesis in NPC.[14] miR-144 has been reported as an oncomiRNA in NPC.[15] In addition, a previous study concluded that miR-144 is one of the inclusions in NPC-cell-derived EVs,[16] but the effect of EV miR-144 on tumor endothelial cells and angiogenesis remains unknown. In the current study, we set out to perform gain- and loss-of-function analyses to determine whether miR-144 shuttled by NPC-derived EVs could elevate human umbilical vein endothelial cell (HUVEC) migration and invasion to ultimately promote angiogenesis.
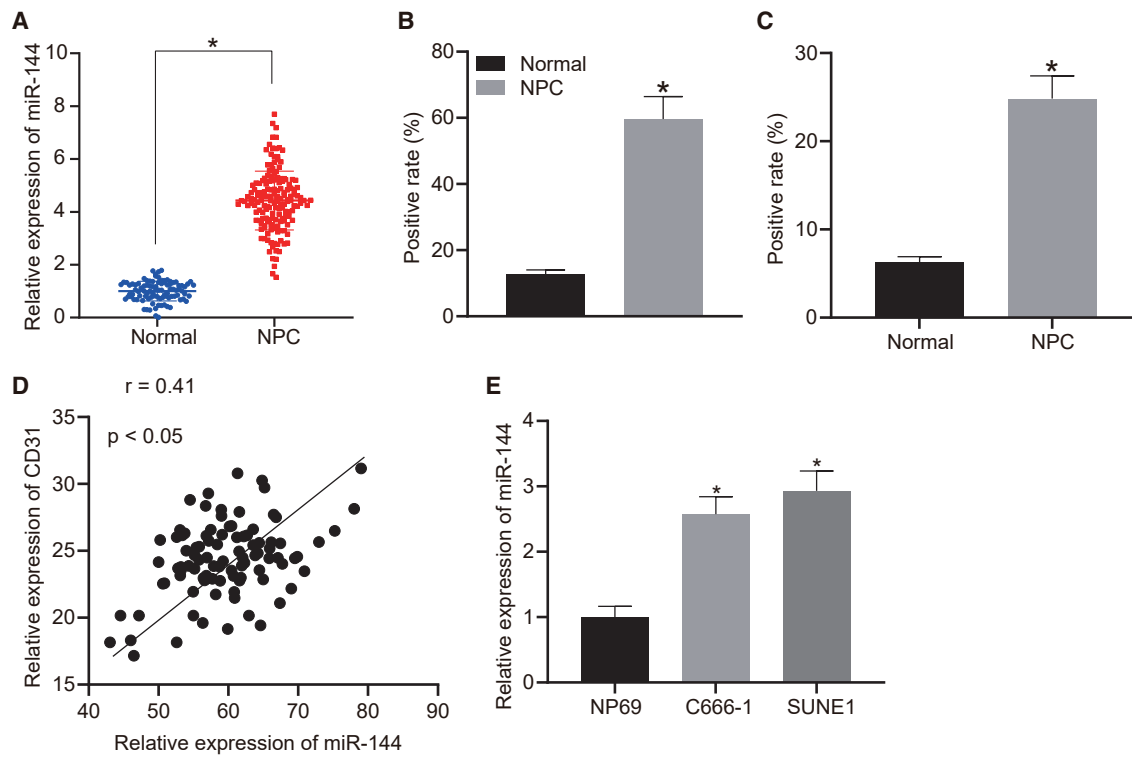
Figure 1. Expression pattern of miR-144 in NPC

(A) The expression of miR-144 compared between NPC biopsy specimens (n = 95) and nasopharyngeal biopsy specimens (n = 95) of chronic nasopharyngitis by qRT-PCR. (B) The expression of miR-144 determined between NPC biopsy specimens (n = 95) and nasopharyngeal biopsy specimens (n = 95) of chronic nasopharyngitis by ISH. (C) Immunohistochemical staining for CD31 of NPC tissues and non-cancerous nasopharyngeal tissues. (D) Correlation between CD31 and miR-144 expression in NPC tissues. (E) The expression of miR-144 compared between human NPC cell lines and a nasopharyngeal epithelial cell line. (A–C) *p < 0.05 compared with non-cancerous nasopharyngeal tissues by unpaired t test. (E) *p < 0.05 compared with NP69 cells by Tukey's-test-corrected one-way ANOVA.
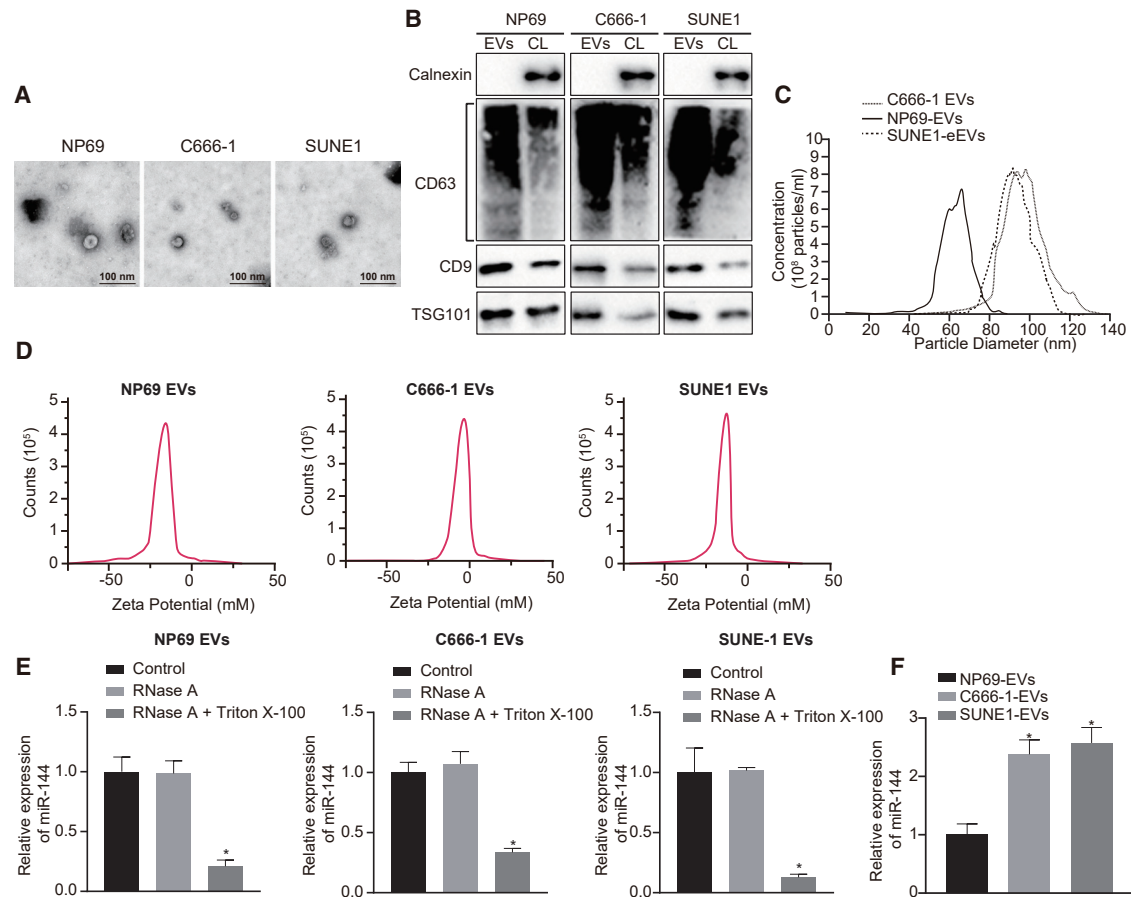
RESULTS

miR-144 is upregulated in NPC tissues and cells

Previous literature has highlighted the cancer-promoting effects of miR-144 during the development of NPC.[15] We initially set out to determine the expression pattern of miR-144 in NPC. The expression of miR-144 was analyzed between 95 NPC biopsy specimens and 95 nasopharyngeal biopsy specimens of chronic nasopharyngitis via quantitative reverse-transcriptase polymerase chain reaction (qRT-PCR). The results obtained indicated that the expression level of miR-144 was higher in the NPC tissues than that in the non-cancerous nasopharyngeal tissues (Figure 1A), which was further verified by *in situ* hybridization (ISH) (Figure 1B). As depicted in Figure 1C, enhanced immunohistochemical staining for CD31 was demonstrated in NPC tissues relative to non-cancerous nasopharyngeal tissues. Moreover, a positive correlation between the expression of CD31 and that of miR-144 was identified in the NPC tissues (Figure 1D). We subsequently compared the expression levels of miR-144 between human NPC cell lines (C666-1 and SUNE1) and a nasopharyngeal epithelial cell line, NP69, via qRT-PCR. As expected, both the C666-1 and SUNE1 cells exhibited higher levels of miR-144 expression relative to NP69 (Figure 1E). These results suggested that miR-144 was highly expressed in NPC tissues and cells, with a positive correlation detected between its expression and that of CD31, highlighting its potential association with tumor angiogenesis.

Highly enriched miR-144 in EVs released from NPC cells

Next, to determine whether tumor-secreted miR-144 has the capacity to influence tumor-microenvironment crosstalk by extracellular communication via EVs, we initially isolated EVs from C666-1, SUNE1, and NP69 cells. The nanoparticle concentration and size distribution of the EVs were examined. Observation under a transmission electron microscope (TEM) revealed that the diameter of nanoparticles ranged from 30 to 100 nm, with each vesicle exhibiting a cup-like shape (Figure 2A). Immunoblotting revealed the presence of common EV-specific markers, including CD9, CD63, and TSG101, with the notable absence of the endoplasmic reticulum membrane protein calnexin in these nanoparticles derived from C666-1, SUNE1, and NP69 cells when compared to corresponding cell lysate (Figure 2B). The nanoparticle tracking analysis (NTA) further revealed that the mean diameter of EVs was 94.1 nm (C666-1 cells), 90.5 nm (SUNE1 cells), and 68.5 nm (NP69 cells), with no difference in EV concentration (Figure 2C). Zeta detected

Figure 2. miR-144 is highly enriched in EVs released from NPC cells

(A) Representative images of TEM for EVs secreted from C666-1, SUNE1, and NP69 cells (scale bar = 100 nm). (B) The presence of CD9, CD63, and TSG101 (common EV-specific markers) immunoblots and the absence of calnexin (endoplasmic reticulum membrane protein) immunoblots of EVs secreted from C666-1, SUNE1, and NP69 cells (EVs, extracellular vesicles; CL, cell lysate). (C) Size distribution and concentration of EVs secreted from C666-1, SUNE1, and NP69 cells. (D) Zeta detection of surface charge of EVs. (E) The expression of miR-144 in EVs from C666-1, SUNE1, and NP69 cells. *p < 0.05 compared with the control group. (F) The expression of miR-144 in EVs secreted from C666-1, SUNE1, and NP69 cells was determined with qRT-PCR. *p < 0.05 compared with NP69-cell-derived EVs by Tukey's-test-corrected one-way ANOVA.

the surface charges of C666-1, SUNE1, and NP69-cell-derived EVs (Figure 2D) in addition to the expression of miR-144 following treatment with varying EVs derived from these three cell lines. The addition of RNase exerted no effect on the expression of miR-144 in the EVs derived from these three cell lines, while the expression of miR-144 was markedly decreased in the cells treated with Triton X-100, indicating that the cell membrane conferred protection on the expression of miR-144 (Figure 2E). The results obtained suggested that EVs from these three cell lines had stable membrane states and exerted protective effects on RNA. The expression of miR-144 was determined in the EVs via qRT-PCR, which revealed the presence of high levels of miR-144 expression in the EVs derived from NPC cells (Figure 2F). These findings provided evidence indicating that miR-144 was upregulated in the NPC-cell-derived EVs.

miR-144 delivery from NPC cells into HUVECs via EVs enhanced HUVEC migration and invasion

Previous literature has provided evidence verifying that endothelial cell migration and tube-forming ability are required for angiogenesis. Hence, we sought to investigate the effect of NPC-EV-secreted miR-144 on HUVEC migration and invasion to elucidate the role of tumor-secreted miR-144 in angiogenesis. Initially, the uptake of PKH67-labeled EVs by HUVECs at different time points was observed under fluorescence microscopy. The results confirmed the presence of PKH67 signals in the cytoplasm of HUVECs, suggesting that the EVs had been endocytosed by HUVECs. As time elapsed, the HUVECs in the C666-1-EV group and the SUNE1-EV group progressively exhibited a significantly greater degree of EV internalization when compared with the NP69-EV group (Figure 3A). qRT-PCR results indicated that the expression of miR-144 was higher in HUVECs
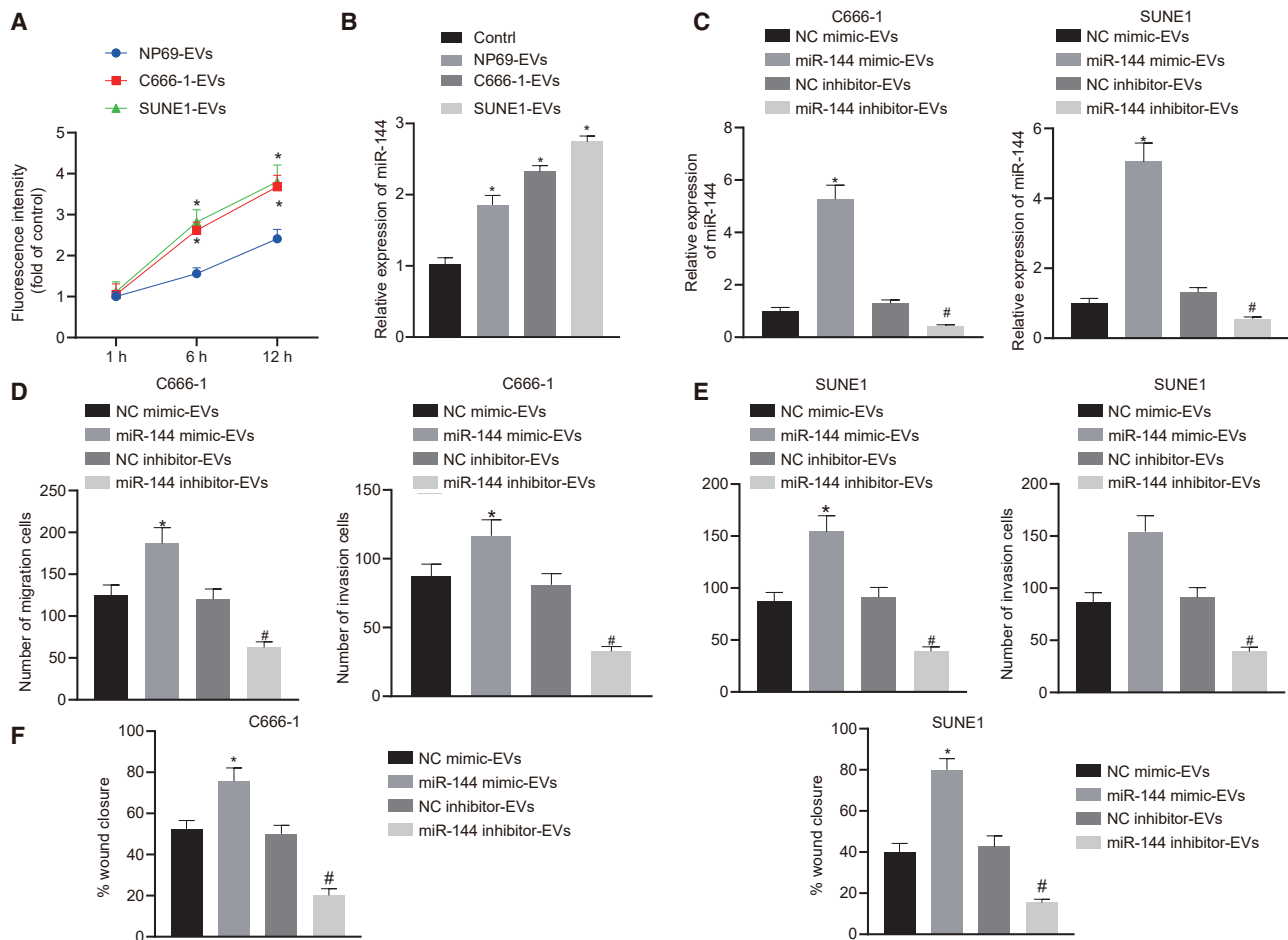
Figure 3. miR-144 is delivered from NPC cells into HUVECs via EVs and enhances HUVEC migration and invasion

(A) miR-144 delivery from NPC cells into HUVECs via EVs at 1, 6, and 12 h. PKH67 signals are localized in the cytoplasm of HUVECs (green). Nuclear counterstaining was performed using DAPI (blue). (B) The expression of miR-144 in HUVECs exposed to EVs released from C666-1, SUNE1, and NP69 cells. (C) The expression of miR-144 in HUVECs exposed to miR-144-interferenced C666-1 and SUNE1 cells. (D) The migration and invasion of HUVECs exposed to EVs from miR-144-interferenced C666-1 cells. (E) The migration and invasion of HUVECs exposed to EVs from miR-144-interferenced SUNE1 cells. (F) The migration of HUVECs exposed to EVs from miR-144-interferenced C666-1 or SUNE1 cells. (B) *$p < 0.05$ compared with HUVECs exposed to EVs from NP69 cells by Tukey's-test-corrected one-way ANOVA. (C–F) *$p < 0.05$ by unpaired t test relative to HUVECs exposed to EVs from miR-mimic NC-treated NPC cells; #$p < 0.05$ by unpaired t test relative to HUVECs exposed to EVs from miR-inhibitor NC-treated NPC cells.

exposed to EVs released from C666-1 and SUNE1 relative to the HUVECs exposed to EVs from NP69 cells (HUVECs not exposed to EVs were used as negative control [NC]) (Figure 3B). To further demonstrate the effects associated with EV miR-144 secreted by NPC cells on endothelial cells, C666-1 and SUNE1 cell lines were transfected, followed by EV extraction. The obtained EVs were co-cultured with HUVECs and grouped into the NC mimic-EV group, miR-144 mimic-EV group, NC inhibitor-EV group, and miR-144 inhibitor-EV group. The qRT-PCR results illustrated that miR-144 was upregulated in HUVECs exposed to miR-144 mimic-treated NPC cells but downregulated in HUVECs exposed to miR-144 inhibitor-treated NPC cells (Figure 3C). The results of Transwell migration and Matrigel-based invasion assays demonstrated that miR-144-overexpressing EVs were sufficient to enhance HUVEC migration and invasion, with

an opposite trend observed with miR-144-inhibiting EVs (Figures 3D and 3E). In addition, the proliferation and migration ability of HUVECs was also measured by a wound-healing experiment (Figure 3F). The results revealed that the wound-healing rate of the cells in the miR-144 mimic-EV group was elevated when compared with that in the NC mimic-EV group, indicating that both C666-1- and SUNE1-cell-derived EV miR-144 promoted the proliferation and migration of HUVECs. The wound-healing rate of cells was diminished in the miR-144 inhibitor-EV group relative to that of the NC inhibitor-EV group, suggesting that the proliferation and migration of HUVECs were inhibited secondary to the inhibition of C666-1- and SUNE1 cell EV miR-144 (both $p < 0.05$). Ultimately, the results obtained provided evidence suggesting that delivery of EV miR-144 to endothelial cells promoted their proliferation and migration.
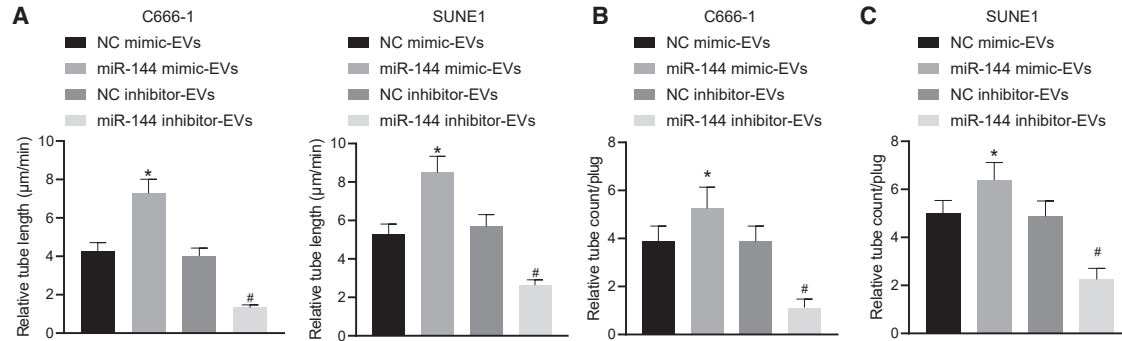
Figure 4. NPC-EVs enhance vessel-like tube formation of HUVECs *in vitro* and *in vivo* via transferring miR-144

(A) The number of vessel-like tubes formed *in vitro*. (B) Neovessels in the transplanted gel plugs containing EVs from C666-1 cells. (C) Neovessels in the transplanted gel plugs containing EVs from SUNE1 cells. *p < 0.05 by unpaired t test relative to HUVECs or transplanted gel plugs containing EVs from miR-mimic NC-treated NPC cells; #p < 0.05 by unpaired t test relative to HUVECs or transplanted gel plugs containing EVs from miR-inhibitor NC-treated NPC cells. n = 8 for each mouse group.

NPC-EVs enhance vessel-like tube formation of HUVECs *in vitro* and *in vivo* via transferring miR-144

We subsequently set out to evaluate the effects associated with NPC-EV-derived miR-144 on vessel-like tube structures of HUVECs to elucidate the role of tumor-secreted miR-144 in angiogenesis. The *in vitro* Matrigel-based angiogenesis assays (Figure 4A) demonstrated notably promoted vessel-like tube formation of HUVECs *in vitro* in the EVs from miR-144 mimic-treated NPC cells, which was a contrasting finding in comparison to the EVs from miR-144 inhibitor-treated NPC cells. Next, to further demonstrate the pro-angiogenic activity of NPC-EV-derived miR-144, an *in vivo* Matrigel plug assay was performed to identify the newly formed blood vessels in the transplanted gel plugs in nude mice (Figures 4B and 4C). We identified that newly formed enhanced blood vessels in the gel plugs were enhanced by EVs from miR-144 mimic-treated NPC cells but reduced by EVs from miR-144 inhibitor-treated NPC cells, which was consistent with the results of the *in vitro* Matrigel-based angiogenesis assays. Based on the aforementioned results, NPC-EV-shuttled miR-144 enhanced vessel-like tube formation of HUVECs both *in vitro* and *in vivo*.

Elevated miR-144 results in downregulation of FBXW7 and upregulation of HIF-1α

Recent research has indicated that FBXW7 plays an important role in vascular endothelial cell migration and inflammation and endothelial barrier integrity and angiogenesis.[17] We subsequently set out to elucidate the molecular mechanisms responsible for the pro-angiogenic function of miR-144 in NPC. The *in-silico* analysis predicted the presence of miR-144 binding sites in the 3′ UTR of FBXW7 mRNA (Figure 5A), which was further confirmed by the reduction detected in luciferase activity at the promoter of the reporter gene containing wild-type (WT) instead of mutant (MUT) 3′ UTR of FBXW7 following co-transfection with miR-144 mimic (Figure 5B). The expression of FBXW7 was compared between NPC tissues and non-cancerous nasopharyngeal tissues at the mRNA level (qRT-PCR) and protein level (immunoblotting). As depicted in Figures 5C and 5D, the mRNA and protein expression of FBXW7 was lower in NPC tissues when compared to the non-cancerous nasopharyngeal

tissues. Pearson's correlation analysis revealed a significant negative correlation between miR-144 expression and FBXW7 expression in NPC tissues (Figure 5E). We also identified a decrease in the degree of immunohistochemical staining for FBXW7 in NPC tissues relative to non-cancerous nasopharyngeal tissues (Figure 5F). Expectedly, both the C666-1 and SUNE1 cells exhibited lower mRNA and protein expression levels of FBXW7 when compared to NP69 cells (Figures 5G and 5H). Previous evidence revealed that the FBXW7/HIF-1α/vascular endothelial growth factor A (VEGF-A) pathway was involved in tumor angiogenesis.[18] Hence, we hypothesized that the pro-angiogenic function of miR-144 was achieved via modulation of the FBXW7/HIF-1α/VEGF-A pathway during carcinogenesis. In the present study, we initially determined FBXW7 and HIF-1α at the mRNA level (qRT-PCR) and protein level (immunoblotting) in HUVECs exposed to EVs from NPC cells with introduction of miR-144 mimic or inhibitor, while VEGF-A concentration in the supernatant of HUVECs was determined with enzyme-linked immunosorbent assay (ELISA) (Figures 5I and 5J). The results obtained revealed diminished expression of FBXW7 in the EVs exposed to miR-144 mimic but increased the expression of HIF-1α and VEGF-A concentration in the supernatant of the HUVECs. Expectedly, the introduction of miR-144 inhibitor led to an increase in FBXW7 expression but reduced HIF-1α expression in the EVs, with a decrease in VEGF-A concentration in the supernatant of the HUVECs detected. Furthermore, we performed a gain-of-function study using pcDNA vector inserted with wild-type FBXW7 fragments and loss-of-function analysis using HIF-1α-specific small interfering RNA (siRNA) in C666-1, SUNE1, and HUVECs. Overexpression of FBXW7 or silencing of HIF-1α led to a reduction in the expression of HIF-1α and VEGF-A concentration in the supernatant of the HUVECs (Figures 5K and 5L). Therefore, miR-144 could target FBXW7 and promote the expression of HIF-1α and VEGF-A.

miR-144 exerts pro-angiogenic function by the FBXW7/HIF-1α/VEGF-A pathway

We subsequently set out to determine whether NPC-EV-derived miR-144 facilitated vessel-like tube formation of HUVECs *in vitro*
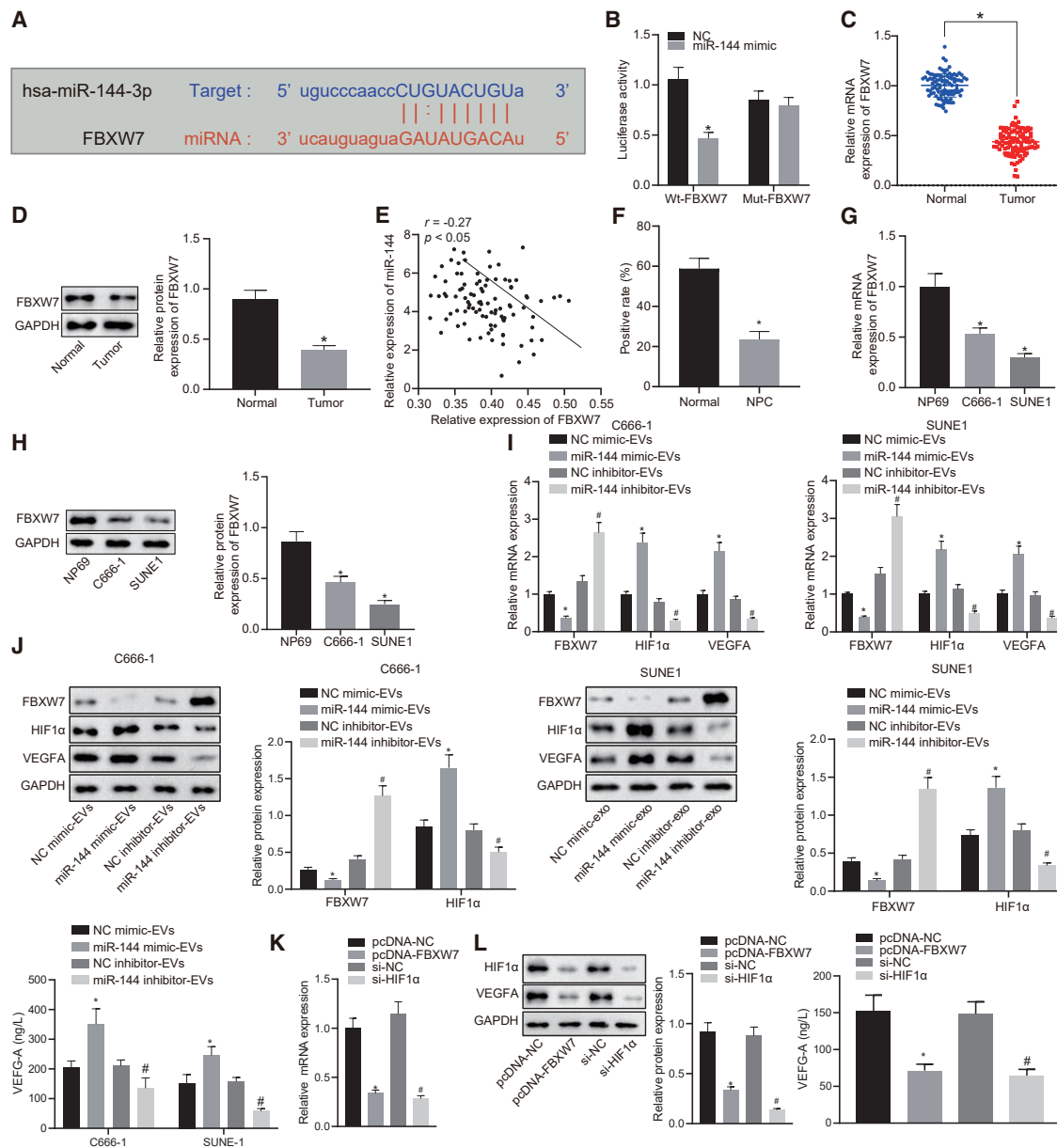
Figure 5. Elevated miR-144 results in downregulation of FBXW7 and upregulation of HIF-1α

(A) The predicted miR-144 binding sites in the 3′ UTR of FBXW7 mRNA. (B) The targeting relationship between miR-144 and FBXW7. *p < 0.05 compared with miR-mimic NC by unpaired t test. (C and D) The expression of FBXW7 in NPC tissues and non-cancerous nasopharyngeal tissues at the mRNA level and protein level. *p < 0.05 compared with non-cancerous nasopharyngeal tissues by unpaired t test. (E) Correlation between the expression of FBXW7 mRNA and miR-144 in NPC tissues. (F) Immunohisto-chemical staining for FBXW7 of NPC tissues and non-cancerous nasopharyngeal tissues. (G) The expression of FBXW7 in C666-1, SUNE1, and NP69 cells at the mRNA level. (H) The expression of FBXW7 in C666-1, SUNE1, and NP69 cells at the protein level. *p < 0.05 compared with NP69 cells by Tukey's-test-corrected one-way ANOVA. (I) The mRNA expression of FBXW7 and HIF-1α. (J) The protein expression of FBXW7 and HIF-1α was determined by immunoblotting in HUVECs, and VEGF-A concentration in the supernatant of HUVECs was determined with ELISA. *p < 0.05 by unpaired t test relative to HUVECs exposed to EVs from miR-mimic NC-treated NPC cells; #p < 0.05 by unpaired t test relative to HUVECs exposed to EVs from miR-inhibitor NC-treated NPC cells. (K) The mRNA expression of FBXW7 and HIF-1α. (L) The protein expression of HIF-1α determined by immunoblotting and VEGF-A concentration in the supernatant of HUVECs were determined with ELISA. *p < 0.05 by unpaired t test relative to treatment of empty pcDNA vector; #p < 0.05 by unpaired t test relative to treatment of scramble siRNA.
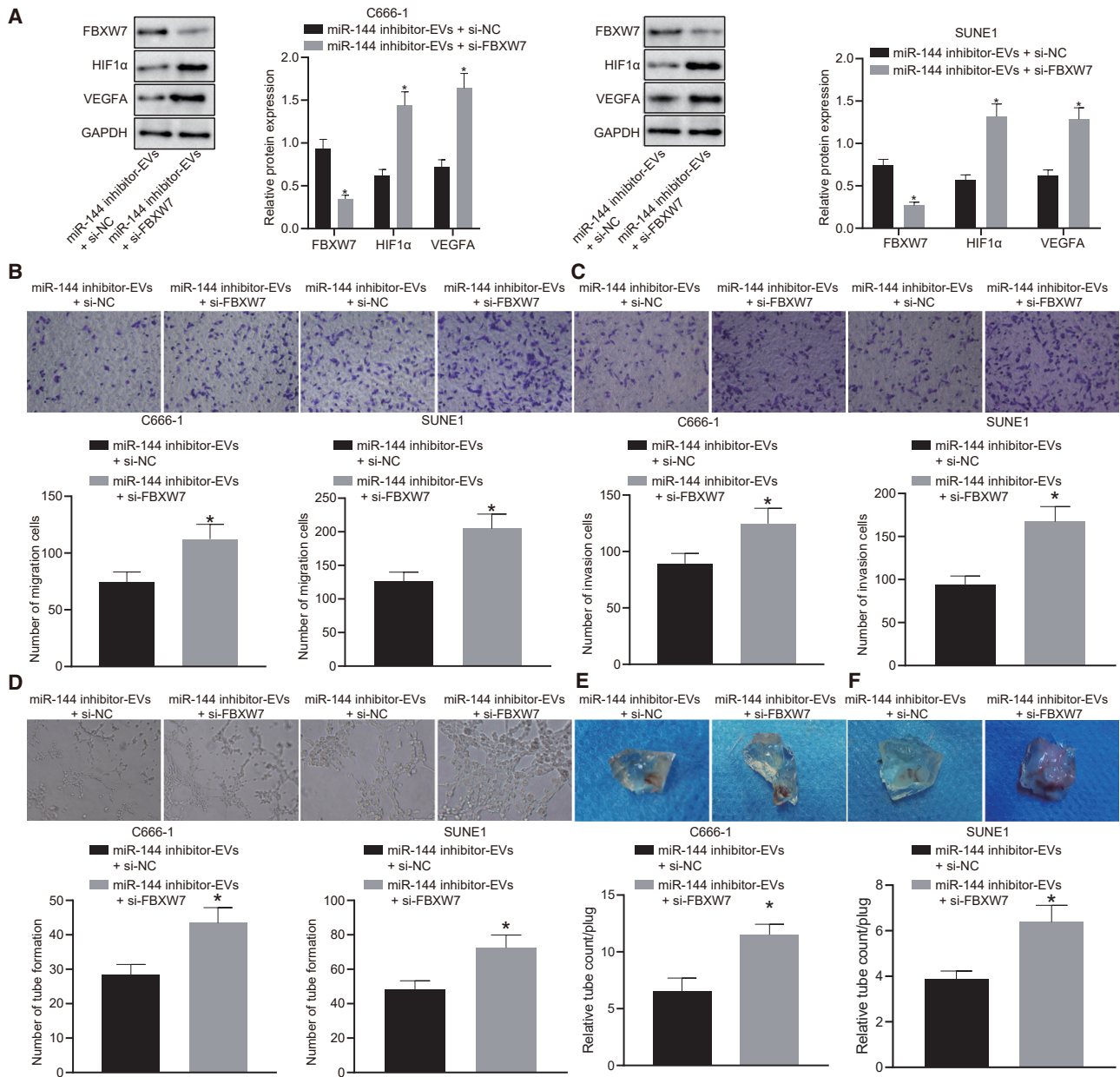
Figure 6. miR-144 exerts pro-angiogenic function by the FBXW7/HIF-1α/VEGF-A pathway *in vivo* (n = 8)

(A) Western blot analysis of FBXW7, HIF-1α, and VEGF-A protein expression. (B) HUVECs migrating from upper Transwell chambers into lower ones. (C) HUVECs invading from Matrigel-coated upper Transwell chambers into lower ones. (D) The number of vessel-like tubes formed *in vitro*. (E) Transplanted gel plugs containing EVs from C666-1. (F) Transplanted gel plugs containing EVs from SUNE1 cells. *p < 0.05 compared with the presence of both EVs from miR-144 inhibitor-treated NPC cells and scramble siRNA by unpaired t test. n = 8 for each mouse group.

and *in vivo* by mediating the FBXW7/HIF-1α/VEGF-A pathway. HUVECs exposed to EVs from miR-144 inhibitor-treated C666-1 and SUNE1 cells were transfected with FBXW7-specific siRNA. As evidenced by the immunoblotting analysis findings, treatment with si-FBXW7 led to a downregulation in the expression of FBXW7 along with elevated HIF-1α and VEGF-A expression in the presence of EVs

derived from miR-144 inhibitor-treated NPC cells, suggesting that the effects of miR-144 on the HIF-1α/VEGF-A pathway took place in a FBXW7-dependent manner (Figure 6A). Likewise, we also identified enhanced HUVEC migration (Figure 6B) and invasion (Figure 6C), as well as increased vessel-like tube formation (Figure 6D) in HUVECs in response to miR-144 inhibition and siRNA knockdown of FBXW7

in combination when compared to miR-144 inhibition alone, which was indicative of the pro-angiogenic function of miR-144 *in vitro* dependent on FBXW7. As we expected, the *in vivo* Matrigel plug assay (Figures 6E and 6F) displayed the gel plugs containing EVs from miR-144 mimic-treated NPC cells possessed enhanced newly formed blood vessels in response to miR-144 inhibition and siRNA knockdown of FBXW7 in combination when compared to miR-144 inhibition alone, recognizing the pro-angiogenic function of NPC-EV miR-144 *in vivo* dependent on FBXW7.

DISCUSSION

Accumulating evidence continues to emphasize the clinical and biological significance of NPC-derived EVs to tumor progression mediation. The crucial role of EVs in a wide variety of malignancies highlights their potential functions as biomarkers and therapeutic targets.[19,20] Hence, the current study set out to investigate the functional interaction of NPC-cell-derived EV-shuttled miR-144 with FBXW7 in relation to NPC tumorigenesis and angiogenesis. Collectively, the experimental data provided evidence suggesting that miR-144 carried by EVs derived from NPC cells contributed to angiogenesis of HUVECs via the upregulation of HIF-1α and VEGF-A through target inhibition of FBXW7, which has the potential to be applied in the development of therapeutic strategies.

A key finding made during the current study revealed high levels of miR-144 expression in NPC tissues and cells as well as in NPC-EVs. Previous reports have highlighted the strong tumorigenic role of miR-144 in NPC, as evidenced by the frequent upregulation of miR-144 in the NPC samples and cells, while malignant cellular behaviors have been reported to be notably suppressed following the repression of miR-144.[15] In addition, knockdown of miR-144 can induce significantly more human type 1 NPC cells to be arrested during the S phase, indicative of cell apoptosis inhibition.[21] Notably, miR-144 has been identified in EVs derived from NPC TW03 and NP69 cell lines as revealed by microarray analysis in a previous report.[16] During the current study, we detected that miR-144 was located in NPC-cell-derived EVs characterized by significantly high levels of expression. Furthermore, microscopic observations provided verification of the internalization of miR-144 by HUVECs. For exploration purposes, the expression of miR-144 in the NPC cells was knocked down using a miR-144 inhibitor. EVs were isolated and co-cultured with HUVECs to ascertain the resulting effects on migration, invasion, and angiogenesis of HUVECs. Based on the findings, HUVEC migratory, invasive, and angiogenic properties were significantly restrained in the presence of EVs harboring miR-144 inhibitor, as evidenced by the diminished levels of HIF-1α and VEGF-A concentration. The HIF-1α/VEGF-A axis has been emphasized as a crucial component of angiogenesis in multiple malignancies.[22–24] As a critical regulator of tumor aggressiveness, HIF-1α promotes proliferation, invasion, and neoangiogenesis and has been implicated in regard to the pro-metastatic effects mediated by EVs in NPC.[25] Activation of HIF-1α has been shown to enhance tumorigenesis of NPC cells via crosstalk with long non-coding RNA cancer susceptibility candidate 9.[26] Moreover, elevated expression of VEGF has been

linked with poor oncological outcomes in patients with NPC.[27] Notably, EVs derived from NPC cells have been reported to enhance angiogenesis by promoting HUVEC migration and invasion,[28] indicating the need for future research efforts to determine the optimal dose for optimal application.

Further investigation into the underlying mechanism revealed that FBXW7 was targeted by miR-144 and was required for the role of miR-144 contained in EVs secreted from NPC cells. Moreover, FBXW7 has been reported to exhibit marked reductions in its expression in NPC tissues and cells and formed an inverse relationship with miR-144. FBXW7 represents a key mediator in human tumorigenesis through its effect on the regulation of diverse cellular pathways, which strongly highlights its potential for application in the development of novel therapeutic approaches.[29] In the context of NPC, FBXW7 has been proposed as a tumor suppressor by means of promoting the drug sensitivity of NPC cells.[30] Importantly, the silencing of FBXW7 has been reported to possess the capacity to neutralize the suppressive effects induced when miR-144 is silenced, which was further evidenced by the results obtained from function assays in the current study. A similar regulatory mechanism has been previously reported in breast cancer, which suggested that upregulation of miR-182 can induce angiogenesis and enhance invasiveness and tumorigenicity accompanied by higher expression levels of HIF-1α and VEGF-A, all of which are offset by ectopic FBXW7 expression, a target gene of miR-182,[16] which indicated that multiple miRNAs can indeed regulate angiogenesis in tumor cells by regulating target genes.

Conclusions

In conclusion, the key findings of the current study provide evidence demonstrating that EV-derived miR-144 serves as a facilitator in the progression of NPC *in vitro*. Specifically, miR-144 could be shuttled to HUVECs via EVs derived from NPC cells, which ultimately strengthens their malignant phenotypes, providing a new target for the development of EV-based biomarkers and treatment modalities against NPC. The mechanistic illustration of pro-angiogenic function of tumor-secreted miR-144 in NPC is depicted in Figure 7. However, further investigations are required to determine whether sustained delivery of NPC-EVs can yield more powerful pro-angiogenic effects and the dose of EVs secreted from tumor cells to endothelial cells residing at close or distant sites *in vivo*. In addition to EVs derived from NPC cell lines, tissue-derived EVs from NPC patients are encouraged to be delivered into orthotopic or metastatic NPC *in vivo*. Further investigation is required in order to determine the feasibility of NPC-EVs as a therapeutic tool for NPC.

MATERIALS AND METHODS
Ethics statement
All study participants provided signed informed consent documentation prior to enrollment into the study. All study protocols were approved by the ethics committee of the Second Affiliated Hospital of Nanchang University. All animal experiments were performed in strict accordance with the approval of the institutional animal care
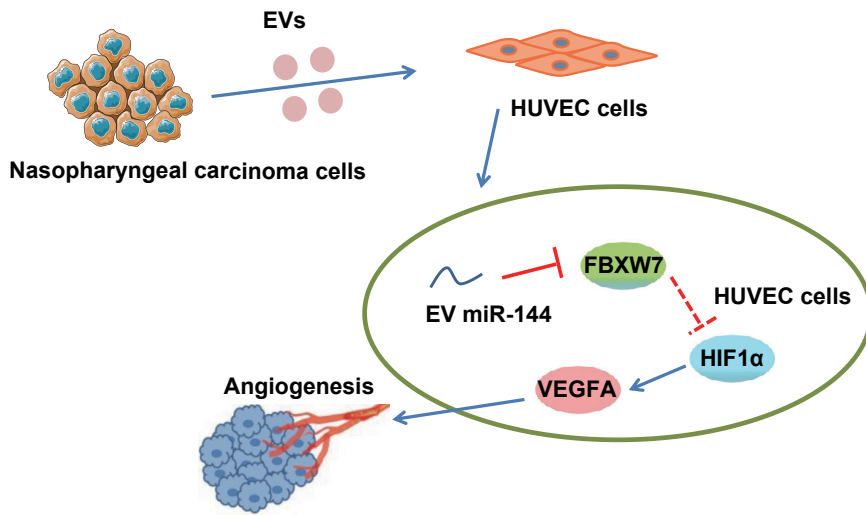
Figure 7. The mechanistic illustration of pro-angiogenic function of tumor-secreted miR-144 in NPC

EVs secreted from NPC cells stimulate tumor angiogenesis via transferring miR-144. miR-144 negatively regulates FBXW7 and thus increases the activity of HIF-1α. Increased HIF-1α promotes the translation of VEGF-A, thereby facilitating endothelial cell migration and tube-forming ability.

and use committee of the Second Affiliated Hospital of Nanchang University.

Clinical samples

Human tumor biopsy specimens were collected from 95 patients (62 males and 33 females; aged 28–61 years) who had been diagnosed with NPC based on histopathological findings at the Second Affiliated Hospital of Nanchang University from June 2016 to October 2018. All patients were yet to receive any therapy prior to biopsy collection. Nasopharyngeal biopsy specimens obtained from 95 patients (66 males and 29 females; aged 28–72 years) with chronic nasopharyngitis served as the control specimens.

RNA extraction and quantification

Total RNA was extracted using a RNeasy Mini Kit (QIAGEN, Valencia, CA, USA). Synthesis of cDNA from mRNA was generated using a commercial kit (RR047A, Takara, Japan) and performed based on the instructions provided by the manufacturer. Synthesis of cDNA of miR-144 was conducted using miRNA First Strand cDNA Synthesis (Tailing Reaction) kit (B532451-0020) as per the instructions provided by the manufacturer (Sangon Biotech, Shanghai, China). cDNA was subject to qRT-PCR using SYBR Premix Ex Taq II (Perfect Real Time) kit (DRR081, Takara, Japan) using an ABI 7500 instrument (Applied Biosystems, Foster City, CA, USA), with each reaction performed in triplicate. The universal RT primer of miRNA and forward primer of U6 were provided by the miRNA First Strand cDNA Synthesis kit. The individual miRNA-specific forward primer and mRNA primer information is listed in Table S1. The miR-144 level was normalized to U6 and the target mRNA level to glyceraldehyde-3-phosphate dehydrogenase (GAPDH). The results were determined using the $2^{-\Delta\Delta CT}$ method.

Immunohistochemical staining and ISH

Paraffin-embedded NPC tissues were cut into 5 μm sections. The sections were made into slides and then immunostained for CD31 and FBXW7. Immunohistochemical staining for CD31, an endothelial cell marker, was performed to identify angiogenesis in the NPC tissues. The number of CD31-positive vessels (1:100 dilution, Abcam, Cambridge, UK) was recorded in 10 random fields of view at 200× magnification. In accordance with the aforementioned, the expression of FBXW7 was examined in NPC tumor samples with the use of immunohistochemical staining. All antibodies were purchased from Abcam. The *in-situ* detection of miR-144 was identified in formalin-fixed paraffin-embedded samples using ISH optimization kits (Exiqon, Vedbaek, Denmark) with miRCURY LNA miR-144 probe, and scramble-miR probe (Exiqon) was used as a NC.

Cell culture

Human NPC cell lines C666-1, SUNE1, and HUVECs were purchased from the Shanghai Institute of Nutrition and Health, Chinese Academy of Sciences and a human immortalized nasopharyngeal epithelial cell line NP69 from BeNa Culture Collection (Beijing, China). C666-1 and SUNE1 cells were grown by the Roswell Park Memorial Institute (RPMI)-1640 (Hyclone, Laboratories, Logan, UT, USA) in the presence of 10% heat-inactivated fetal bovine serum (FBS, Gibco, Gaithersburg, MD, USA), HUVECs in the 10% FBS-contained endothelial basic medium (EBM-2), and NP69 cells in the Keratinocyte-SFM (Invitrogen, Carlsbad, CA, USA) in the presence of bovine pituitary extract (BD Biosciences, Sparks, MD, USA). All cells were cultured under controlled conditions at 37°C in a 5% CO_2-containing atmosphere.

Transient transfection

The NPC cells as well as the HUVECs were seeded in either 6-well or 96-well plates 24 h prior to transfection commencement. Transient transfection of miR-144 mimic (50 nM), miR-144 inhibitor (100 nM), NC mimic (50 nM), and NC inhibitor (100 nM) (all from Ambion, Austin, TX, USA) was performed using Lipofectamine 2000 reagent (Invitrogen).

Transient transfection of siRNAs (Invitrogen) against FBXW7 and HIF-1α and si-NC (100 nM) was performed using 0.5% (v/v) Lipofectamine 2000 to inhibit the expression of FBXW7 and HIF-1α. The siRNA stock solution was formulated into 20 μM solution by RNase-free water. Cell culture medium was replaced with Opti-MEM

I reduced serum medium (Invitrogen). Next, siRNAs were transfected into cells using Lipofectamine 2000 as per the instructions provided. FBXW7 siRNA or HIF-1α siRNA at a concentration of 100 nM prepared with 0.5% (v/v) lipid carrier was transfected into cells in 2 mL Opti-MEM medium in each well of the standard 6-well plate in preparation for subsequent experiments.

To overexpress FBXW7, HUVECs (2×10^6 cells/mL) were transfected with pcDNA-FBXW7 plasmid vector (500 μg), and the plasmid containing FBXW7 was provided by GenePharma (Shanghai, China). Upon reaching 90% confluence of the HUVECs to the culture plate, pcDNA-FBXW7 was transfected into the cells in accordance with the instructions of the Lipofectamine 2000 kit (Invitrogen). HUVECs transfected with pcDNA-NC were used as controls. The cells were cultured at 37°C for 3 days for subsequent experiments.

Characterization of EVs released from NPC cells
The cell culture medium was subsequently subjected to differential centrifugation at $300 \times g$, $1,200 \times g$, and $10,000 \times g$ for 3 h followed by 3-h ultracentrifugation at $110,000 \times g$ (all procedures performed at 4°C). The EVs were collected from the pellet and subsequently resuspended using phosphate-buffered saline (PBS). The morphologies of EVs were observed under a TEM (H-7650, Hitachi, Japan) at 80 kV acceleration voltage. The particle diameter and concentration were measured with NTA using the Nanosight NS3000 system (Nanosight, Amesbury, UK). The characteristic surface marker proteins CD9, CD63, and TSG101 and the endoplasmic reticulum membrane protein, calnexin, of EVs were determined using immunoblotting. Surface charge (ζ electric potential) of different cell EV particles was analyzed with the use of Zetasizer Nano series Nano-ZS (Malvern Instruments, Malvern, UK).

Detection of miRNAs in EVs to evaluate EV stability
RNAase treatment was employed to ascertain whether the miRNAs were surface bound to or packaged in EVs. Next, 10 μg EVs were resuspended in PBS with the incubation conducted using 10 μg/μL RNase (Purelink RNase A, Life Technologies, Carlsbad, CA, USA) for 20 min at 37°C. In addition, the specificity of the miRNAs was determined by disrupting vesicle membrane integrity using 0.3% Triton X-100 treatment, followed by 20-min treatment with radio-immunoprecipitation assay (RIPA) buffer and RNase treatment in accordance with the aforementioned steps. After incubation with RNase A, lysis buffer was supplemented to inhibit the reaction, and RNA was isolated for TaqMan miRNA analysis. The relative expression of miR-144 was determined based on the comparison with and without RNase A (10 μg/mL) and/or 0.3% Triton X-100 treatment.

Uptake of PKH67-labeled EVs
The isolated EVs were labeled using the green lipophilic fluorescent dye PKH67 (Sigma-Aldrich, St. Louis, MO, USA) and maintained with HUVECs. The labeled EVs were then incubated with cultured HUVECs. After incubation for 1, 6, and 12 h, uptake of PKH67-labeled EVs by HUVECs was traced under a confocal microscope (FV10i, Olympus, Tokyo, Japan), with 4′6-diamidinophenylidole (DAPI, Abbott, Abbott Park, IL, USA) used for nuclear staining.

Luciferase assay
FBXW7 dual-luciferase reporter vector and mutant (400 ng) on binding sites of miR-144 were constructed, namely PGLO-FBXW7 wild-type and PGLO-FBXW7 mutant type. The reporter plasmids were subsequently co-transfected with miR-144 mimic and NC mimic into HEK293T cells (the final concentration of 50 nM; 1×10^6 cells/mL). The cells were lysed 24 h post transfection and centrifuged at $4,000 \times g$ for 1 min, after which the supernatant was collected. The luminescence of firefly luciferase was determined using a Dual-Luciferase Reporter Assay System (E1910, Promega, Madison, WI, USA). Firefly luciferase activity was detected following the addition of 100 μL firefly luciferase working fluid to each cell sample (1×10^6 cells/mL), and Renilla luciferase activity was measured by adding 100 μL Renilla luciferase working fluid. The ratio of firefly luciferase activity to Renilla luciferase activity was regarded as the relative luciferase activity.

Transwell migration and Matrigel-based invasion assays
Transwell chambers (Corning, Corning, NY, USA) with 24-well (8 μm) plates were employed for the subsequent experiment. Briefly, HUVECs were cultured using serum-free RPMI-1640 medium with 200 μL of HUVECs (5×10^5 cells/mL) added to the apical chambers and treated with EVs at the concentration of 0.2 μg/μL (600 μL EVs/well) from differently transfected NPC cells. In the lower chamber, 600 μL complete medium (Invitrogen) containing 10% FBS was added as chemokine. Following incubation of the chamber at 37°C with 5% CO_2 for 48 h, the chamber was fixed with 4% paraformaldehyde for 30 min, treated with 0.2% Triton X-100 (Sigma) for 15 min, and stained with 0.05% crystal violet for 5 min. The stained cells were determined from five random fields in each well using an inverted microscope (XDS-800D, Shanghai Caikang Optical, China). The cell migration and invasion assay procedures were performed in an identical fashion, with the exception of the use of 50 μL Matrigel (Sigma-Aldrich) in the invasion assays.

Wound-healing experiment
The effects of the different conditional treatments on endothelial cell proliferation and migration were determined by wound healing. HUVECs (1×10^5 cells/well) were seeded into 12-well plates. After 24 h, two vertical wounds were formed using a 1 mL pipette tip. Following treatment with EVs at a concentration of 0.2 μg/μL (600 μL EVs/well) from differentially transfected NPC cells, HUVECs were treated with EGM-2 growth medium containing 2% FBS at 37°C with 5% CO_2. Images were captured at 10× magnification at 0 h and 12 h. Three different areas of the wound were measured using ImageJ software. The vertical distance between the wounds at 0 h and 12 h was compared, with the wound closure rates expressed as a percentage of the difference between the wound-healing distance at the two different time points/the initial post-injury distance.

Matrigel-based angiogenesis assays

Initially, the Matrigel was removed and melted. The Matrigel was diluted with culture medium at a ratio of 1:1. Next, the diluted Matrigel was evenly spread on the cell culture plate in the absence of bubbles. The Matrigel plate was solidified at 37°C for 1 h. HUVECs were maintained in the plate coated by Matrigel (300 μL/well) at 2×10^4 cells/well and treated with EVs (600 μL EVs/well) from differentially transfected NPC cells for 24 h. The number of tubular structures formed by HUVECs was subsequently determined under a microscope (a complete closed loop was regarded as a tubular structure), which was considered to be indicative of angiogenesis. The formation of vessel-like tube structures was quantitated as the mean relative tube length based on 5 random microscopic views using ImageJ software.

In vivo Matrigel plug assays

HUVECs (4×10^6) were incubated with EVs derived from 2×10^6 C666-1 or SUNE1 cells and then made into cell suspension. Cell suspension and 500 μL growth-factor-reduced Matrigel (BD Matrigel 356230) were then mixed at ratio of 1:1. Next, 500 μL Matrigel was subsequently injected subcutaneously into the dorsal region of 96 BALB/c mice (female, aged 4–6 weeks, weighing 18–22 g) (8 mice for each group). Briefly, a small skin mound was made by injecting air on the back of the mouse, and Matrigel was injected into the skin mound. The plugs were collected, and angiogenesis was evaluated and observed 2 weeks later. The number of tubular structures formed in each Matrigel plug (a complete closed loop was regarded as a tubular structure) was evaluated to determine angiogenesis.

Protein extraction and quantification

Protein extraction was performed using protease-inhibitor-contained RIPA buffer (R0010, Solarbio, Beijing, China). The protein sample was separated using freshly prepared SDS-PAGE, electro-transferred onto polyvinylidene fluoride (PVDF) membranes, and probed with primary antibodies (Abcam, Cambridge, UK). Immunoblots were visualized with goat anti-rabbit IgG (1:10,000, ab205718) and enhanced chemiluminescence detection reagents and captured using a SmartView Pro 2000 (UVCI-2100, Major Science, Saratoga, CA, USA) microscope. Gray value of target protein bands was quantified using Quantity One software, with GAPDH used for normalization. The primary antibodies used were as follows: anti-FBXW7 antibody (ab109617, 1:1,000), anti-HIF-1α antibody (ab51608, 1:2,000), anti-VEGF-A antibody (ab183100, 1:450), anti-CD9 antibody (ab92726, 1:1,000), anti-CD63 antibody (ab217345, 1:1,000), anti-calnexin antibody (ab92573, 1:20,000), and anti-GAPDH antibody (1:1,000, ab22555).

ELISA

After the cell supernatant had been collected, it was centrifuged at 2,000 rpm for 3 min to remove debris. The supernatant was saved as a sample awaiting analysis. The slats were taken out from a sealed bag that had been equilibrated to room temperature. Standard and sample diluent were subsequently added to the blank wells, with samples or standards of different concentrations (100 μL/well) added to the remaining wells. The reaction wells were then sealed using sealing tape and incubated in a 36°C incubator for 90 min. The biotinylated antibody working solution was prepared 20 min in advance. The blank wells were added with biotinylated antibody diluent, while biotinylated antibody working solution (100 μL/well) was added to the remaining wells. The reaction wells were sealed with new sealing tape and incubated at 36°C for 60 min. The enzyme conjugate working solution was prepared 20 min in advance under conditions void of light at 22°C–25°C. Enzyme conjugate diluent was subsequently added to the blank wells, while enzyme conjugate working solution (100 μL/well) was added to the remaining wells, followed by sealing and incubation at 36°C for 30 min under conditions void of light. The microplate reader was warmed up and the detection program was set. 100 μL/well of chromogenic substrate (TMB) was added to the wells and incubated for 15 min under dark conditions in a 36°C incubator. 100 μL/well of stopping solution was added to the wells. The OD450 value (within 3 min) was measured immediately after mixing, after which the concentration of the target substance was determined in the sample.

Statistical analysis

All statistical analyses were completed with SPSS 21.0 software (IBM, Armonk, NY, USA). Data were expressed as the mean ± standard deviation from a minimum of three independent experiments performed in triplicate. Unless otherwise noted, statistical comparisons were performed using an unpaired t test during comparisons between two groups or by Tukey's-test-corrected one-way analysis of variance (ANOVA) when comparing more than two groups. The correlation of measurements was conducted using Pearson's correlation analysis. Two-tailed $p < 0.05$ was considered to be indicative of statistical significance.

SUPPLEMENTAL INFORMATION

Supplemental information can be found online at https://doi.org/10.1016/j.omtn.2021.03.016.

AUTHOR CONTRIBUTIONS

X.Y.T., Y.H.L., Z.W., and S.H.W. designed the study. X.Y.T. collated the data, carried out data analyses, and produced the initial draft of the manuscript. Y.H.L., Z.W., and S.H.W. contributed to drafting the manuscript. All authors have read and approved the final submitted manuscript.

DECLARATION OF INTERESTS

The authors declare no competing interests.

REFERENCES

1. Chen, Y.P., Chan, A.T.C., Le, Q.T., Blanchard, P., Sun, Y., and Ma, J. (2019). Nasopharyngeal carcinoma. Lancet *394*, 64–80.

2. Bray, F., Ferlay, J., Soerjomataram, I., Siegel, R.L., Torre, L.A., and Jemal, A. (2018). Global cancer statistics 2018: GLOBOCAN estimates of incidence and mortality worldwide for 36 cancers in 185 countries. CA Cancer J. Clin. 68, 394–424.

3. Lee, A.W., Ma, B.B., Ng, W.T., and Chan, A.T. (2015). Management of Nasopharyngeal Carcinoma: Current Practice and Future Perspective. J. Clin. Oncol. 33, 3356–3364.

4. Viallard, C., and Larrivée, B. (2017). Tumor angiogenesis and vascular normalization: alternative therapeutic targets. Angiogenesis 20, 409–426.

5. Collet, G., Szade, K., Nowak, W., Klimkiewicz, K., El Hafny-Rahbi, B., Szczepanek, K., Sugiyama, D., Weglarczyk, K., Foucault-Collet, A., Guichard, A., et al. (2016). Endothelial precursor cell-based therapy to target the pathologic angiogenesis and compensate tumor hypoxia. Cancer Lett. 370, 345–357.

6. Xu, Z., Fang, S., Zuo, Y., Zhang, Y., Cheng, R., Wang, Q., Yang, Z., Cai, W., Ma, J., Yang, X., and Gao, G. (2011). Combination of pigment epithelium-derived factor with radiotherapy enhances the antitumor effects on nasopharyngeal carcinoma by downregulating vascular endothelial growth factor expression and angiogenesis. Cancer Sci. 102, 1789–1798.

7. Chen, Z., and Xu, X.H. (2015). Combining antiangiogenic therapy and radiation in nasopharyngeal carcinoma. Saudi Med. J. 36, 659–664.

8. Chen, S., Lv, L., Zhan, Z., Wang, X., You, Z., Luo, X., and You, H. (2020). Silencing of long noncoding RNA SRRM2-AS exerts suppressive effects on angiogenesis in nasopharyngeal carcinoma via activating MYLK-mediated cGMP-PKG signaling pathway. J. Cell. Physiol. 235, 7757–7768.

9. Xing, Z., Zhao, C., Liu, H., and Fan, Y. (2020). Endothelial Progenitor Cell-Derived Extracellular Vesicles: A Novel Candidate for Regenerative Medicine and Disease Treatment. Adv. Healthc. Mater. 9, e2000255.

10. Xavier, C.P.R., Caires, H.R., Barbosa, M.A.G., Bergantim, R., Guimarães, J.E., and Vasconcelos, M.H. (2020). The Role of Extracellular Vesicles in the Hallmarks of Cancer and Drug Resistance. Cells 9, 1141.

11. Servage, K.A., Stefanius, K., Gray, H.F., and Orth, K. (2020). Proteomic Profiling of Small Extracellular Vesicles Secreted by Human Pancreatic Cancer Cells Implicated in Cellular Transformation. Sci. Rep. 10, 7713.

12. Wee, I., Syn, N., Sethi, G., Goh, B.C., and Wang, L. (2019). Role of tumor-derived exosomes in cancer metastasis. Biochim. Biophys. Acta Rev. Cancer 1871, 12–19.

13. Ludwig, N., Yerneni, S.S., Razzo, B.M., and Whiteside, T.L. (2018). Exosomes from HNSCC Promote Angiogenesis through Reprogramming of Endothelial Cells. Mol. Cancer Res. 16, 1798–1808.

14. Bao, L., You, B., Shi, S., Shan, Y., Zhang, Q., Yue, H., Zhang, J., Zhang, W., Shi, Y., Liu, Y., et al. (2018). Metastasis-associated miR-23a from nasopharyngeal carcinoma-derived exosomes mediates angiogenesis by repressing a novel target gene TSGA10. Oncogene 37, 2873–2889.

15. Zhang, L.Y., Ho-Fun Lee, V., Wong, A.M., Kwong, D.L., Zhu, Y.H., Dong, S.S., Kong, K.L., Chen, J., Tsao, S.W., Guan, X.Y., and Fu, L. (2013). MicroRNA-144 promotes cell proliferation, migration and invasion in nasopharyngeal carcinoma through repression of PTEN. Carcinogenesis 34, 454–463.

16. Ye, S.B., Zhang, H., Cai, T.T., Liu, Y.N., Ni, J.J., He, J., Peng, J.Y., Chen, Q.Y., Mo, H.Y., Jun-Cui, et al. (2016). Exosomal miR-24-3p impedes T-cell function by target-ing FGF11 and serves as a potential prognostic biomarker for nasopharyngeal carcinoma. J. Pathol. 240, 329–340.

17. Yang, M., Li, C.J., Sun, X., Guo, Q., Xiao, Y., Su, T., Tu, M.L., Peng, H., Lu, Q., Liu, Q., et al. (2017). MiR-497~195 cluster regulates angiogenesis during coupling with osteogenesis by maintaining endothelial Notch and HIF-1α activity. Nat. Commun. 8, 16003.

18. Chiang, C.H., Chu, P.Y., Hou, M.F., and Hung, W.C. (2016). MiR-182 promotes proliferation and invasion and elevates the HIF-1α-VEGF-A axis in breast cancer cells by targeting FBXW7. Am. J. Cancer Res. 6, 1785–1798.

19. You, B., Shan, Y., Bao, L., Chen, J., Yang, L., Zhang, Q., Zhang, W., Zhang, Z., Zhang, J., Shi, S., and You, Y. (2018). The biology and function of extracellular vesicles in nasopharyngeal carcinoma (Review). Int. J. Oncol. 52, 38–46.

20. Zhou, Y., Xia, L., Lin, J., Wang, H., Oyang, L., Tan, S., Tian, Y., Su, M., Wang, H., Cao, D., and Liao, Q. (2018). Exosomes in Nasopharyngeal Carcinoma. J. Cancer 9, 767–777.

21. Wu, C.W., Wang, S.G., Lin, M.L., and Chen, S.S. (2019). Downregulation of miR-144 by triptolide enhanced p85α-PTEN complex formation causing S phase arrest of human nasopharyngeal carcinoma cells. Eur. J. Pharmacol. 855, 137–148.

22. Liang, H., Xiao, J., Zhou, Z., Wu, J., Ge, F., Li, Z., Zhang, H., Sun, J., Li, F., Liu, R., and Chen, C. (2018). Hypoxia induces miR-153 through the IRE1α-XBP1 pathway to fine tune the HIF1α/VEGFA axis in breast cancer angiogenesis. Oncogene 37, 1961–1975.

23. Wang, J., Man, G.C.W., Chan, T.H., Kwong, J., and Wang, C.C. (2018). A prodrug of green tea polyphenol (-)-epigallocatechin-3-gallate (Pro-EGCG) serves as a novel angiogenesis inhibitor in endometrial cancer. Cancer Lett. 412, 10–20.

24. Kong, J., Kong, J., Pan, B., Ke, S., Dong, S., Li, X., Zhou, A., Zheng, L., and Sun, W.B. (2012). Insufficient radiofrequency ablation promotes angiogenesis of residual hepatocellular carcinoma via HIF-1α/VEGFA. PLoS ONE 7, e37266.

25. Aga, M., Bentz, G.L., Raffa, S., Torrisi, M.R., Kondo, S., Wakisaka, N., Yoshizaki, T., Pagano, J.S., and Shackelford, J. (2014). Exosomal HIF1α supports invasive potential of nasopharyngeal carcinoma-associated LMP1-positive exosomes. Oncogene 33, 4613–4622.

26. Su, X., Li, G., and Liu, W. (2017). The Long Noncoding RNA Cancer Susceptibility Candidate 9 Promotes Nasopharyngeal Carcinogenesis via Stabilizing HIF1α. DNA Cell Biol. 36, 394–400.

27. Pan, J., Tang, T., Xu, L., Lu, J.J., Lin, S., Qiu, S., Chen, G., and K Tham, I.W. (2013). Prognostic significance of expression of cyclooxygenase-2, vascular endothelial growth factor, and epidermal growth factor receptor in nasopharyngeal carcinoma. Head Neck 35, 1238–1247.

28. Lu, J., Liu, Q.H., Wang, F., Tan, J.J., Deng, Y.Q., Peng, X.H., Liu, X., Zhang, B., Xu, X., and Li, X.P. (2018). Exosomal miR-9 inhibits angiogenesis by targeting MDK and regulating PDK/AKT pathway in nasopharyngeal carcinoma. J. Exp. Clin. Cancer Res. 37, 147.

29. Cao, J., Ge, M.H., and Ling, Z.Q. (2016). Fbxw7 Tumor Suppressor: A Vital Regulator Contributes to Human Tumorigenesis. Medicine (Baltimore) 95, e2496.

30. Song, Y., Zhou, X., Bai, W., and Ma, X. (2015). FBW7 increases drug sensitivity to cisplatin in human nasopharyngeal carcinoma by downregulating the expression of multidrug resistance-associated protein. Tumour Biol. 36, 4197–4202.

Supplemental information

miR-144 delivered by nasopharyngeal carcinoma-derived EVs stimulates angiogenesis through the FBXW7/HIF-1α/VEGF-A axis

Xiaoyan Tian, Yuehui Liu, Zhi Wang, and Shuhong Wu

Table S1 Primer sequences used for RT-qPCR.

Target	Primer sequence (5'-3')
miR-144	F: 5'-TACAGTATAGATGATGTACT-3'
FBXW7	F: 5'-GTCCCGAGAAGCGGTTTGATA-3'
	R: 5'-TGCTCGGCACGTCAGAAAAG-3'
HIF1α	F: 5'-AGGTGGATATGTCTGGGTTG-3'
	R: 5'-AAGGACACATTCTCTGTTT-3'
VEGF-A	F: 5'-TGTGATTCTGATAAAATAGACATTGC-3'
	R: 5'-TTTTTCCCCCACAATTATTACG-3'
GAPDH	F: 5'-GCACCGTCAAGGCTGAGAAC-3'
	R: 5'-TGGTGAAGACGCCAGTGGA-3'